

An ALS-associated KIF5A mutant forms oligomers and aggregates and induces neuronal toxicity

Juri Nakano¹ | Kyoko Chiba² | Shinsuke Niwa^{1,2} 

¹Graduate School of Life Sciences, Tohoku University, Sendai, Japan

²Frontier Research Institute for Interdisciplinary Sciences (FRIS), Tohoku University, Sendai, Miyagi, Japan

Correspondence

Kyoko Chiba, Frontier Research Institute for Interdisciplinary Sciences (FRIS), Tohoku University, 6-3 Aramaki-Aoba, Aoba-ku, Sendai, Miyagi 980-0845, Japan.
Email: kyoko.chiba.e7@tohoku.ac.jp

Shinsuke Niwa, Frontier Research Institute for Interdisciplinary Sciences (FRIS), Tohoku University, 6-3 Aramaki-Aoba, Aoba-ku, Sendai, Miyagi 980-0845, Japan.
Email: shinsuke.niwa.c8@tohoku.ac.jp

Funding information

Japan Society for the Promotion of Science, Grant/Award Numbers: 19H04738, 20H03247, 20K21378, 21K20621; Ministry of Education, Culture, Sports, Science & Technology, Grant/Award Number: JPMXS0320200156; Kato Memorial Bioscience Foundation; Takeda Science Foundation; Uehara Memorial Foundation

Communicated by: Gohta Goshima

Abstract

KIF5A is a kinesin superfamily motor protein that transports various cargos in neurons. Mutations in *Kif5a* cause familial amyotrophic lateral sclerosis (ALS). These ALS mutations are in the intron of *Kif5a* and induce mis-splicing of KIF5A mRNA, leading to splicing out of exon 27, which in human KIF5A encodes the cargo-binding tail domain of KIF5A. Therefore, it has been suggested that ALS is caused by loss of function of KIF5A. However, the precise mechanisms regarding how mutations in KIF5A cause ALS remain unclear. Here, we show that an ALS-associated mutant of KIF5A, KIF5A(Δ exon27), is predisposed to form oligomers and aggregates in cultured mouse cell lines. Interestingly, purified KIF5A(Δ exon27) oligomers showed more active movement on microtubules than wild-type KIF5A in vitro. Purified KIF5A(Δ exon27) was prone to form aggregates in vitro. Moreover, KIF5A(Δ exon27)-expressing *Caenorhabditis elegans* neurons showed morphological defects. These data collectively suggest that ALS-associated mutations of KIF5A are toxic gain-of-function mutations rather than simple loss-of-function mutations.

KEYWORDS

aggregation, ALS, KIF5A

1 | INTRODUCTION

Neuronal development, function, and maintenance depend on intracellular transport (Hirokawa et al., 2009). Kinesin superfamily proteins (KIFs) and cytoplasmic dyneins are molecular motors that enable anterograde and retrograde transport, respectively (Hirokawa et al., 2010; Kardon & Vale, 2009). Among KIFs, the Kinesin-1, -2, and -3 family

members are the main anterograde transporters in neurons (Hall & Hedgecock, 1991; Niwa et al., 2008; Okada et al., 1995; Scholey, 2008; Vale et al., 1985; Xia et al., 2003). KIFs generally consist of a conserved motor domain, a dimerized coiled-coil domain, and a cargo-binding tail domain. The motor domain exhibits microtubule-stimulated ATPase activity, which allows the protein to move along microtubules (Hackney, 1995). Each KIF has a specialized tail domain (Vale, 2003) that binds to specific cargo vesicles and protein complexes (Hirokawa et al., 2009).

Juri Nakano and Kyoko Chiba contributed equally to this work.

This is an open access article under the terms of the [Creative Commons Attribution-NonCommercial](https://creativecommons.org/licenses/by-nc/4.0/) License, which permits use, distribution and reproduction in any medium, provided the original work is properly cited and is not used for commercial purposes.

© 2022 The Authors. *Genes to Cells* published by Molecular Biology Society of Japan and John Wiley & Sons Australia, Ltd.

Advances in genomic sequencing technology have allowed identification of many disease-associated mutations in motor protein genes (Hirokawa et al., 2010; Holzbaur & Scherer, 2011). Mutations in KIFs and dynein subunits often cause motor neuron diseases. For example, mutations in Kinesin-3 family members, such

as KIF1A and KIF1B, cause hereditary spastic paraplegia and Charcot-Marie-Tooth disease type 2A1 (Boyle et al., 2021; Budaitis et al., 2021; Chiba et al., 2019; Zhao et al., 2001). Mutations in dynein heavy chain 1 (DYNC1H1) cause Charcot-Marie-Tooth disease type 2O and spinal muscular atrophy-1 (Harms

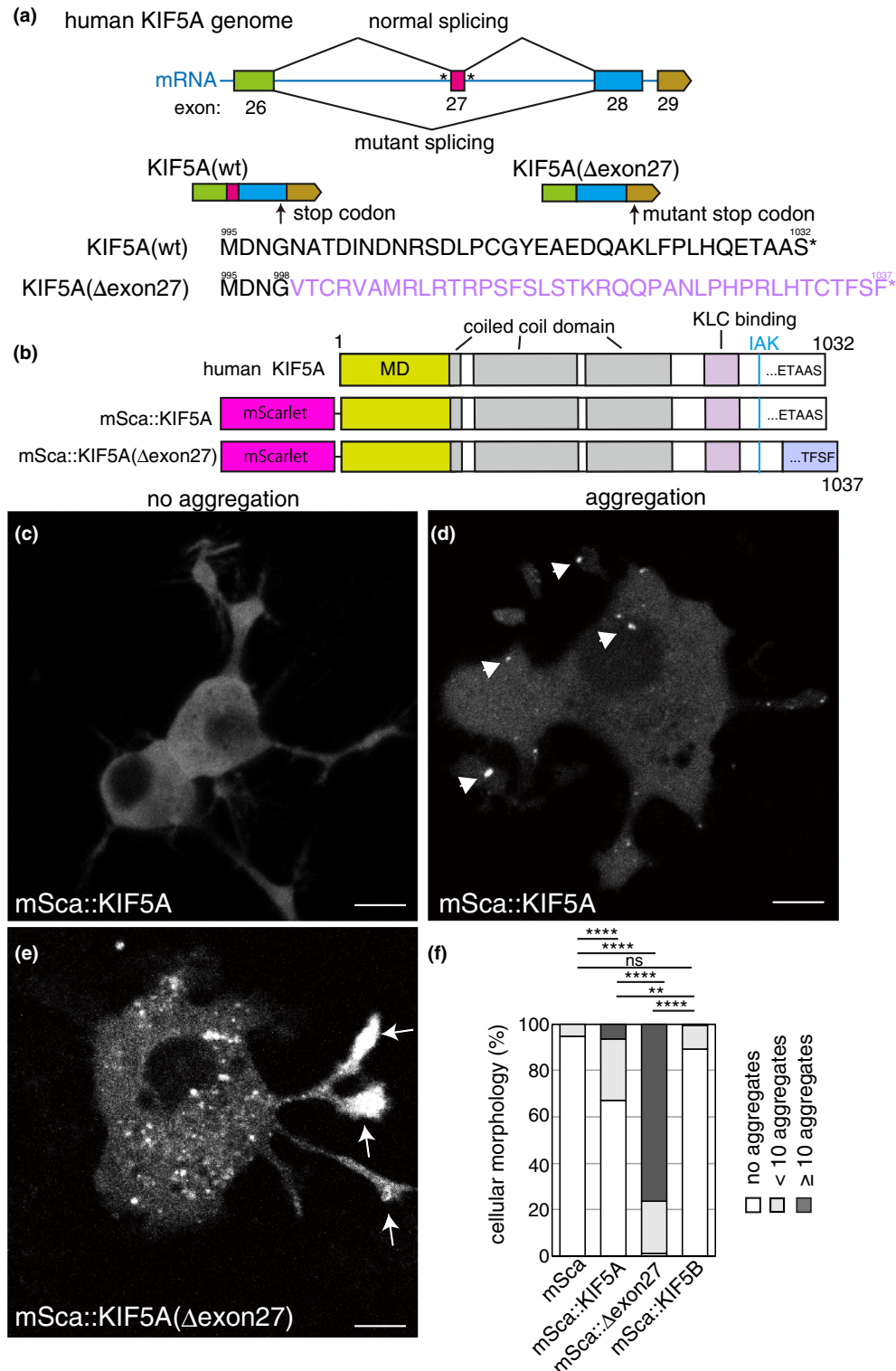


FIGURE 1 Legend on next page.

et al., 2012; Weedon et al., 2011). Mutations in the p150 subunit of dynactin (DCTN1), an activator of dynein, cause amyotrophic lateral sclerosis (ALS; Munch et al., 2004). Gain-of-function mutations in BICD2, a cargo adaptor protein for the cytoplasmic dynein complex, also cause spinal muscular atrophy (Huynh & Vale, 2017). KIF5A mutations are associated with hereditary spastic paraplegia (SPG) and ALS (Brenner et al., 2018; Nicolas et al., 2018; Reid et al., 2002). KIF5A transport protein complexes and membrane organelles such as neurofilaments, RNA granules and mitochondria (Hirokawa et al., 2010; Kanai et al., 2004; Uchida et al., 2009; Xia et al., 2003). The mutated residues differ between KIF5A-associated SPG and ALS. SPG is caused by motor domain mutations in KIF5A that abolish the motor activity of the KIF5A motor (Ebbing et al., 2008). However, ALS-associated KIF5A mutations commonly induce missplicing and deletion of exon 27 (Figure 1a; Brenner et al., 2018; Nicolas et al., 2018). The Δ exon27 mutation induces frameshift, leading to abnormal C-terminal tail (Figure 1a). Previous studies have suggested that ALS-associated mutations in KIF5A are loss-of-function mutations because of the deletion of the cargo-binding tail domain (D. Brenner et al., 2018; Nicolas et al., 2018). However, the precise molecular mechanism of KIF5A-associated ALS has not been shown.

We show here that the product of ALS-associated KIF5A alleles, KIF5A(Δ exon27), is predisposed to form oligomers and aggregates. Binding of KLC1, a cargo adaptor of KIF5A, was not affected by Δ exon27. Interestingly, KIF5A(Δ exon27) oligomers showed higher motility than those of wild-type KIF5A regardless of the presence of KLC1. Furthermore, exogenous expression of KIF5A(Δ exon27) caused defects in the neuronal morphology of *Caenorhabditis elegans*. Collectively, these findings suggest that ALS-associated mutations in

KIF5A are toxic gain-of-function mutations rather than simple loss-of-function mutations.

2 | RESULTS

2.1 | KIF5A(Δ exon27) forms aggregates in the cell

To study the molecular mechanism of ALS caused by KIF5A mutations, we expressed mScarlet-fused KIF5A (mSca::KIF5A) and mScarlet-fused KIF5A(Δ exon27) (mSca::KIF5A(Δ exon27)) in a neuron-like cell line, CAD (Qi et al., 1997; Figure 1b–f). 20 hours after the transfection, mSca::KIF5A was mostly diffuse throughout the cell, but approximately 30% of mSca::KIF5A-expressing cells showed small aggregates in the cytoplasm (Figure 1c–f), which is consistent with our prior finding showing a propensity of KIF5A to form oligomers (Chiba et al., 2022). The proportion of cells showing aggregation was increased compared with cells expressing mScarlet-fused KIF5B, a homologue of KIF5A (Hirokawa et al., 2009). Only 10% of mSca::KIF5B-expressing cells exhibited aggregates. In contrast, mSca::KIF5A(Δ exon27) formed many aggregates in the cytoplasm, as noted in 97% of cells. We observed that aggregates often accumulated in the tip of neurites in CAD cells (Figure 1e arrows), which is similar to the localization of KIF5A with constitutive-active mutations (Nakata et al., 2011). Few aggregates were found in mScarlet-expressing cells (Figure 1f). Formation of aggregates is not due to the higher expression of mSca::KIF5A(Δ exon27) because most mSca::KIF5A(Δ exon27)-expressing cells had aggregates even 6 h after the transfection. These data suggest that KIF5A is predisposed to form aggregates in the cell and that the ALS-associated mutation Δ exon27 strongly enhances aggregate formation.

FIGURE 1 Cellular distribution of amyotrophic lateral sclerosis (ALS)-associated KIF5A mutations. (a) Schematic drawing of ALS mutations in KIF5A. ALS-associated KIF5A mutations (asterisks) are often found in introns around exon 27 and commonly induce missplicing of exon 27 and frameshifts. Amino acid sequences show the C-terminal sequences of wild type KIF5A (black font) and KIF5A (Δ exon27) (purple font). (b) Schematic drawing showing mScarlet-fused wild-type KIF5A (mSca::KIF5A) and mScarlet-fused mutant KIF5A (mSca::KIF5A(Δ exon27)). Motor domain (MD) (1–335 a.a.), coiled-coil domains (331–374 a.a., 408–539 a.a. and 632–800 a.a.), light chain binding domain (KLC binding) (822–905 a.a.) and IAK motif (918–920 a.a.), that is required for the autoinhibition, are shown. (c–f) mSca::KIF5A and mSca::KIF5A(Δ exon27) were expressed in CAD cells and analyzed by fluorescence microscopy. (c and d) Representative images showing the localization of mSca::KIF5A (c and d) and mSca::KIF5A(Δ exon27) (e). Arrow heads and arrows indicate cytoplasmic aggregates and aggregates accumulated to neurite tips, respectively. Bars, 10 μ m. (f) The cells were classified by the mScarlet signal distribution into three categories: no aggregates (white), no more than 10 aggregates (light gray) and more than 10 aggregates (dark gray), and the number of cells in each category was counted. $N = 98$ mScarlet-expressing cells, 112 KIF5A(wt)-expressing cells, 101 KIF5A (Δ exon27)-expressing cells, and 177 KIF5B-expressing cells. A chi-square test with Bonferroni correction was used for data analysis. ns, adjusted p value $>.05$ and not statistically significant. *, adjusted p value $<.05$. **, adjusted p value $<.01$. **** adjusted p value $<.0001$

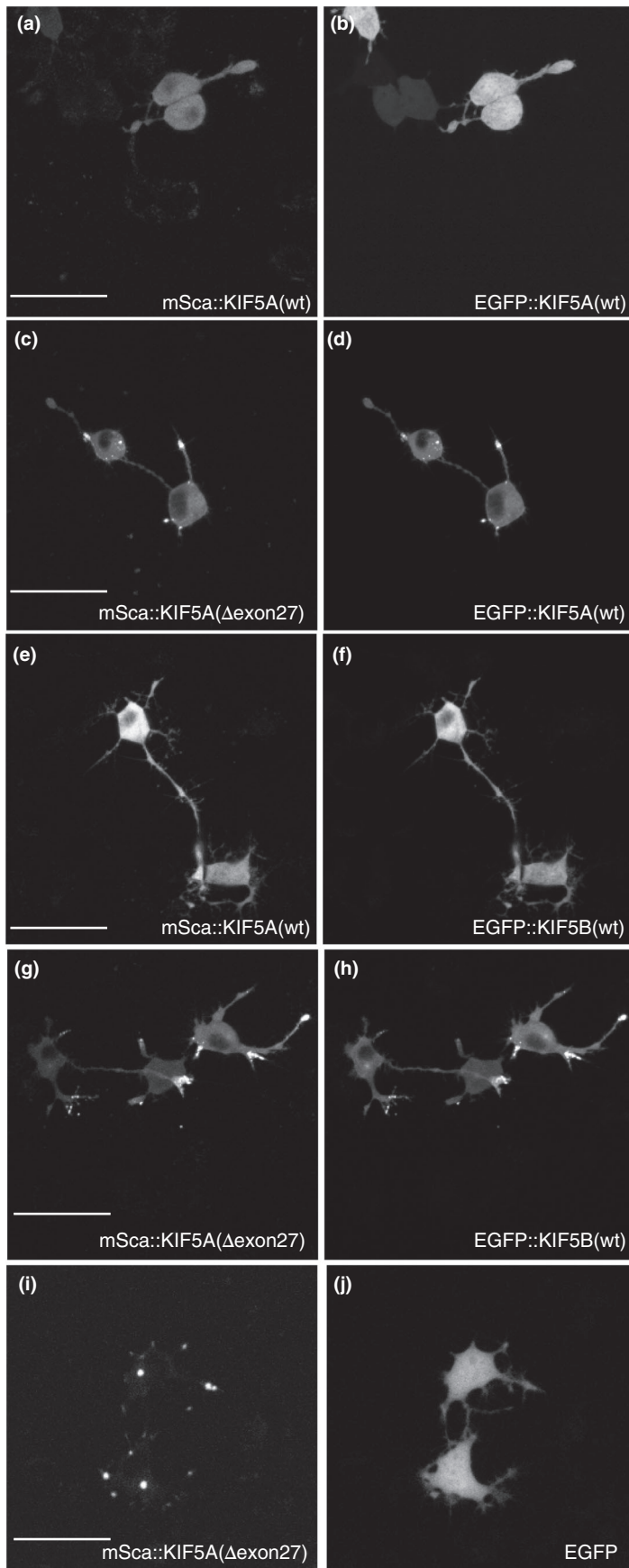


FIGURE 2 Co-aggregation of amyotrophic lateral sclerosis-associated KIF5A. mScarlet fused to KIF5A or KIF5A (Δ exon27) was co-expressed with enhanced green fluorescent protein (EGFP)-fused proteins in CAD cells. (a and b) Representative images showing mSca::KIF5A (a) and EGFP::KIF5A (b) co-expressing cells. When mSca::KIF5A did not form aggregates, EGFP::KIF5A did not co-aggregate in the same cell. No cells (0/70) showed co-aggregation. (c and d) Representative images showing mSca::KIF5A(Δ exon27) (c) and EGFP::KIF5A (d) co-expressing cells. Note that EGFP::KIF5A co-aggregated with mSca::KIF5A(Δ exon27). All cells (85/85, 100%) showed co-aggregation. (e and f) Representative images showing mSca::KIF5A (e) and EGFP::KIF5B (f) co-expressing cells. When mSca::KIF5A did not form aggregates, EGFP::KIF5B did not co-aggregate as well. No cells (0/70) showed co-aggregation. (g and h) Representative images showing mSca::KIF5A(Δ exon27) and EGFP::KIF5B co-expressing cells. Note that EGFP::KIF5B co-aggregated with mSca::KIF5A(Δ exon27). All cells (82/82, 100%) showed co-aggregation. (i and j) Representative images showing mSca::KIF5A(Δ exon27) and EGFP co-expressing cells. Even when mSca::KIF5A(Δ exon27) formed aggregates in the cytoplasm, no GFP aggregation was observed. No cells (0/54) showed co-aggregation. Bars, 50 μ m

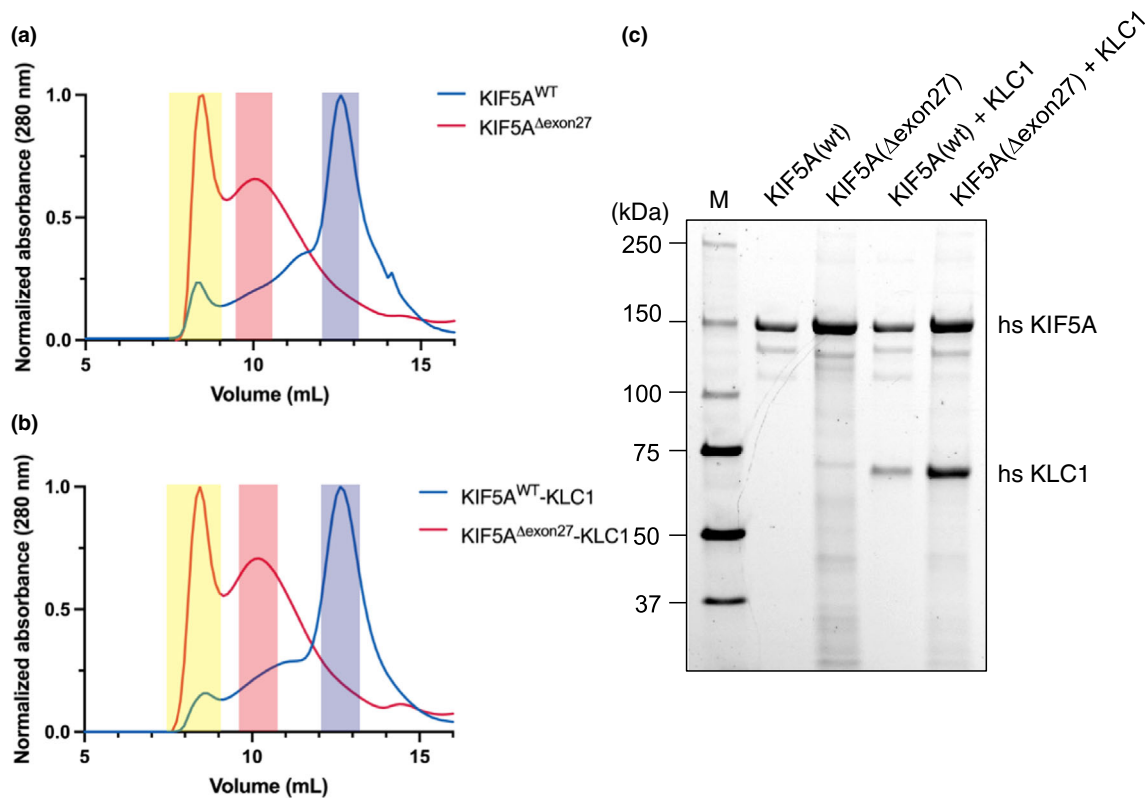


FIGURE 3 Purification of KIF5A and KIF5A(Δ exon27). mScarlet was added to the C-terminus of either KIF5A (KIF5A::mSca) or KIF5A(Δ exon27) (KIF5A(Δ exon27)::mSca). Recombinant proteins were expressed in sf9 cells and then purified. (a and b) Normalized size exclusion chromatograms for KIF5A::mSca and KIF5A(Δ exon27)::mSca (a) and KIF5A::mSca-KLC1 and KIF5A(Δ exon27)::mSca-KLC1 (b). The yellow shaded area shows the void volume of the column corresponding to potential aggregates, the red shaded area shows the fraction corresponding to oligomers, and the blue shaded area shows the fraction corresponding to KIF5A dimers or KIF5A-KLC1 tetramers. (c) Coomassie blue stained gel showing purified KIF5A::mSca, KIF5A(Δ exon27)::mSca, KIF5A::mSca-KLC1, and KIF5A(Δ exon27)::mSca-KLC1. Wild-type protein from the blue shaded fraction and Δ exon27 protein from the red shaded fraction (a and b) were analyzed.

2.2 | KIF5A(Δ exon27) co-aggregates with wild-type motors

We investigated whether the ALS-associated KIF5A protein co-aggregates with wild-type motors. mSca::KIF5A(Δ exon27) was co-expressed with enhanced green fluorescent protein (EGFP)-labeled KIF5A (EGFP::KIF5A). Previous studies have shown that KIF5A forms a homodimer and moves along microtubules (Hackney, 1995; Hackney et al., 1991; Vale et al., 1996). As expected, mSca::KIF5A(Δ exon27) co-aggregated with EGFP::KIF5A(wt) in the cell (Figure 2a–d), and aggregates accumulated at the tips of CAD cell neurites. *Homo sapiens* have three homologous kinesin heavy chain genes: KIF5A, KIF5B, and KIF5C (Hirokawa et al., 2009). These three proteins are highly conserved but do not form heterodimers (Kanai et al., 2000). Interestingly, mSca::KIF5A(Δ exon27) co-aggregated with EGFP::KIF5B(wt) (Figure 2e–h). However, EGFP::KIF5B was diffuse in the cytoplasm when mSca::KIF5A did not form aggregates (Figure 2e,f), and EGFP::KIF5B(wt) uncharacteristically accumulated in neurite tips and co-aggregated with mSca::KIF5A(Δ exon27) (Figure 2g,h). In

contrast, mSca::KIF5A(Δ exon27) did not co-aggregate with EGFP alone (Figure 2i,j). These data suggest that KIF5A(Δ exon27) co-aggregates with wild-type KIF5A and KIF5B motors in the cell.

2.3 | KIF5A(Δ exon27) oligomerizes in vitro

Kinesin-1 is a heterotetramer composed of two heavy chains (KIF5) and two light chains (KLC; Hackney et al., 1991). We have previously shown that KIF5A has a propensity to form oligomers in vitro (Chiba et al., 2022). To examine the effect of the Δ exon27 mutation on the interaction of KIF5A with KLC1 and oligomerization, we next purified heavy chain dimers (KIF5A) and Kinesin-1 tetramers (KIF5A-KLC1) with or without the Δ exon27 mutation. First, we expressed full-length KIF5A::mSca and KIF5A(Δ exon27)::mSca in sf9 cells and purified them by affinity chromatography and size exclusion chromatography (SEC; Chiba et al., 2022). In SEC, wild-type KIF5A predominantly eluted at a single peak (Figure 3a,

blue shaded area). In addition, a small amount of wild-type KIF5A was recovered from fractions that were eluted before the major peak and from the void volume (Figure 3a, red and yellow shaded areas). SEC coupled with multi angle light scattering (SEC-MALS) analyses have shown that the main peak corresponds to KIF5A dimers and that the minor peak eluted before the main peak represents KIF5A oligomers (Chiba et al., 2022). Next, we examined KIF5A(Δ exon27) and found that the Δ exon27 mutation markedly changed the elution profile from that of wild-type KIF5A. The major elution peak of Δ exon27 shifted toward a higher molecular weight, which corresponds to oligomerization (Figure 3a, red shaded area). Most KIF5A(Δ exon27) was recovered from high molecular weight fractions but not from dimer fractions. Thus, the Δ exon27 mutation induces oligomerization of KIF5A. We note that Δ exon27 also increased the population recovered from the void volume, suggesting the potential of KIF5A(Δ exon27) to form aggregates as well as oligomers (Figure 3a, yellow shaded area).

Next, to determine whether binding of the KLC subunit is affected, we co-expressed KLC1 with full length KIF5A or KIF5A(Δ exon27). KLC1 was co-purified either with KIF5A(wt) or KIF5A(Δ exon27) (Figure 3b,c). The ratio of heavy chains to light chains was almost 1:1 and was not markedly affected by Δ exon27. Thus, binding to KLC is not abolished by the deletion of exon 27. The KIF5A-KLC1 complex showed an elution profile similar to that of KIF5A in the SEC analysis (Figure 3b, blue lines). With KIF5A(Δ exon27)-KLC1, we again observed a peak shifted toward a higher molecular weight and an increased population recovered from the void volume. These results suggest that the propensity of KIF5A(Δ exon27) to form oligomers and aggregates is not largely affected by KLC1.

2.4 | KIF5A(Δ exon27) oligomers are hyperactivated on microtubules

We analyzed the motility of purified microtubule motors at single-molecule resolution by total internal reflection fluorescence microscopy (Chiba et al., 2019; Chiba et al., 2022; McKenney et al., 2014). Purified full-length KIF5A(wt)::mSca and KIF5A(wt)::mSca-KLC1 did not bind or move well on microtubules (Figure 4a,b) because of the autoinhibitory mechanism described previously (Chiba et al., 2022; Coy et al., 1999; Friedman & Vale, 1999; Hackney & Stock, 2000). In contrast, we found that full-length KIF5A(Δ exon27)::mSca and full-length KIF5A(Δ exon27)::mSca-KLC1 frequently bound to and moved along microtubules (Figure 4a-c). KLC1 suppresses the binding of KIF5A(Δ exon27) onto microtubules

(Figure 4c). Interestingly, Δ exon27 mutation did not delete the IAK motif that is essential for the autoinhibitory mechanism of kinesin heavy chains (Figure 1b; Coy et al., 1999; Friedman & Vale, 1999; Hackney & Stock, 2000). The fluorescent intensities of KIF5A(Δ exon27)::mSca and full-length KIF5A(Δ exon27)::mSca-KLC1 were stronger than those of KIF5A(wt)::mSca and KIF5A(wt)::mSca-KLC1 (Figure 4b), suggesting the formation of oligomers. On average, the binding rates of KIF5A(Δ exon27)::mSca and KIF5A(Δ exon27)::mSca-KLC1 were nine times higher than those of KIF5A(wt)::mSca and KIF5A(wt)::mSca-KLC1, respectively (Figure 4c). We previously showed that the average run length and velocity of wild-type KIF5A are 1.0 μ m and 1.1 μ m/s, respectively (Chiba et al., 2022); however, we could not collect a sufficient number of samples to measure the run length and velocity of wild-type proteins under the present condition. The median run lengths of KIF5A(Δ exon27)::mSca and KIF5A(Δ exon27)::mSca-KLC1 were approximately 3 μ m each (Figure 4d), which is much longer than that of wild-type KIF5A. No significant difference was detected between KIF5A(Δ exon27)::mSca and KIF5A(Δ exon27)::mSca-KLC1. The velocity of KIF5A(Δ exon27)::mSca and KIF5A(Δ exon27)::mSca-KLC1 was 0.4 μ m/s (Figure 4e,f), which is slower than that of wild-type KIF5A. Taken together, these results suggest that KIF5A oligomers induced by Δ exon27 are more active than those of wild-type KIF5A both in the presence and absence of the KLC subunit (Table 1).

2.5 | KIF5A(Δ exon27) oligomers tend to form aggregates

To examine the properties of KIF5A(Δ exon27), we incubated purified mScarlet, KIF5A::mSca and KIF5A(Δ exon27)::mSca at 37°C and measured the turbidity of protein solutions by determining the optical density at 600 nm, which was used to monitor the formation of protein aggregates in solution in a previous study (Schafheimer & King, 2013). Immediately before incubation, protein solutions were centrifuged and clarified. The turbidity of purified KIF5A(Δ exon27)::mSca increased gradually while those of mScarlet and KIF5A::mSca did not (Figure 5a). Twenty-four hours later, the solution was again centrifuged, and purified mSca::KIF5A(Δ exon27) formed a protein pellet (Figure 5b). At this concentration, purified mScarlet and KIF5A::mSca did not form visible pellets at all, even after the 24-h incubation. These data indicate that purified KIF5A(Δ exon27) is predisposed to form protein aggregates in vitro.

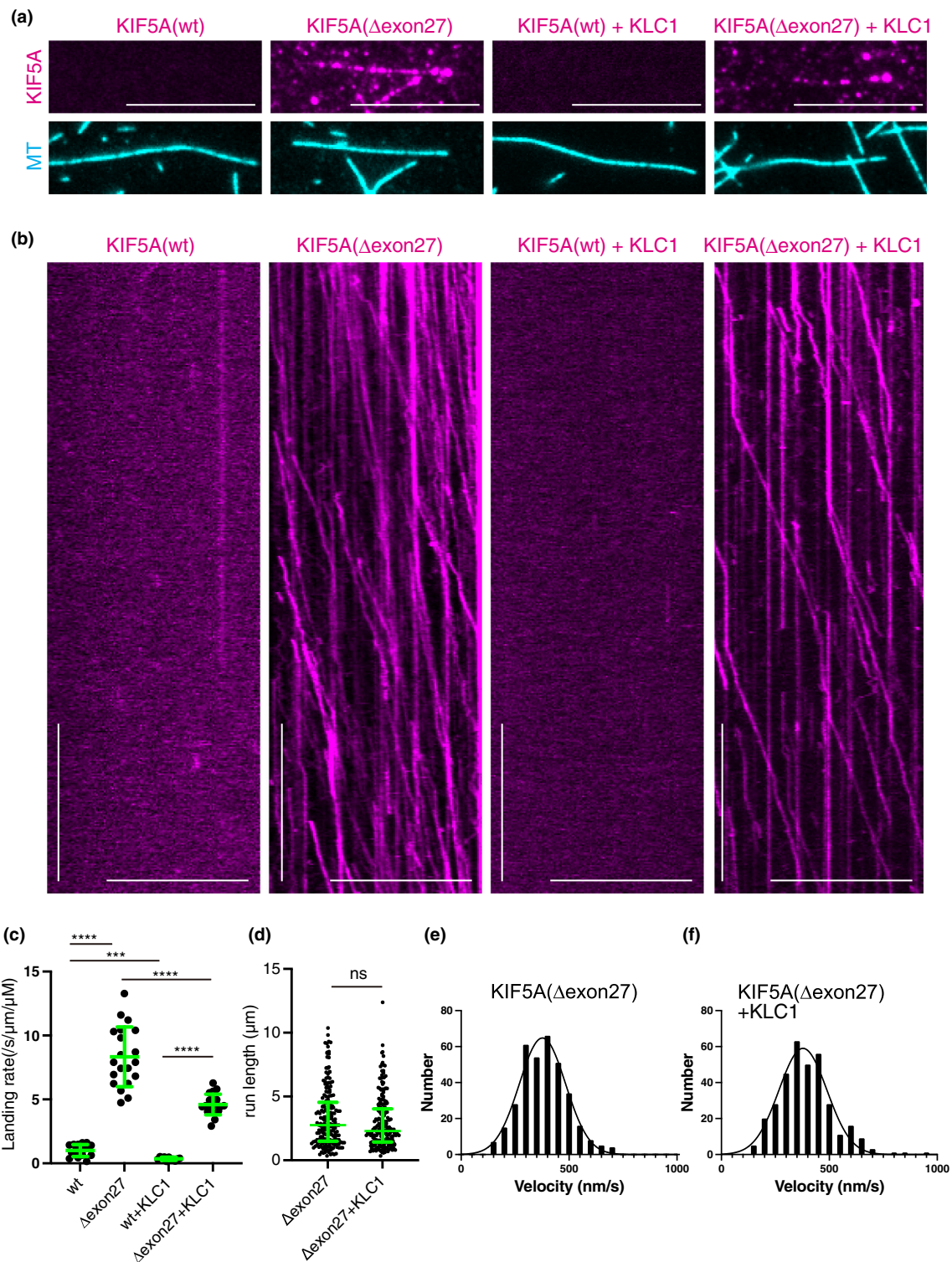


FIGURE 4 Legend on next page.

2.6 | KIF5A(Δ exon27) is toxic in *Caenorhabditis elegans* neurons

Previous studies have shown that ALS is caused by toxic gain-of-function mutations (Bruijn et al., 1998; Johnson et al., 2009; Kwiatkowski Jr. et al., 2009). Therefore, we

examined the toxicity of KIF5A(Δ exon27) in *C. elegans* neurons. The morphology of mechanosensory neurons was compared after expressing human KIF5A and KIF5A (Δ exon27) (Figure 6a–f). Mechanosensory neurons were analyzed because many studies have shown that these neurons have very stereotypical morphology and show

TABLE 1 Measured parameters of KIF5A

Summary of motility measurement of KIF5A(Δ exon27)				
		Velocity (nm/s)	Landing rates (motors/ μ m/s/ μ m)	Run length (μ m)
KIF5A(1–420)		1048 \pm 173 ^a	162 \pm 31 ^a	0.70 ^a (0.55–0.93)
Full-length KIF5A	Wild-type	1182 \pm 187 ^a	0.85 \pm 0.57	1.00 ^a (0.69–1.61)
	Δ exon27	377 \pm 107	8.3 \pm 2.3	2.76 (1.50–4.54)
KIF5A-KLC1 complex	Wild-type	1051 \pm 176 ^a	0.20 \pm 0.20	1.49 ^a (0.78–2.84)
	Δ exon27	378 \pm 111	4.6 \pm 0.80	2.30 (1.44–4.03)

Note: The motility parameters of tail-truncated KIF5A(1–420), full-length KIF5A and KIF5-KLC1 complex. Velocities (mean \pm SD), landing rates (mean \pm SD), and run lengths (median and interquartile range) are shown.

^aValues are described in Chiba et al. (2022).

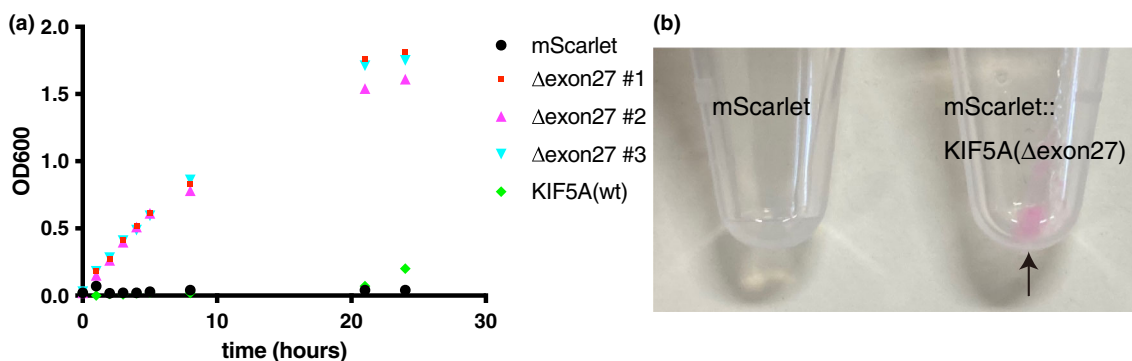


FIGURE 5 Aggregate formation in vitro. Purified mScarlet, KIF5A::mSca or KIF5A(Δ exon27)::mSca (1 μ M) was incubated at 37°C. (a) Turbidity of the solution. The optical density of samples was measured at a wavelength of 600 nm (OD600) and plotted at the indicated time points. Results from three independent experiments are shown for KIF5A(Δ exon27)::mSca. (b) After 24 h of incubation, the samples were centrifuged at 18,000 g for 10 min, and the presence of a pellet was detected. Note that a protein pellet was induced in the KIF5A (Δ exon27)::mSca sample, while no pellet was observed in purified mScarlet

small variations in the wild-type background (Gallegos & Bargmann, 2004; Ghosh-Roy et al., 2012). The morphology of posterior lateral microtubule (PLM) and posterior

ventral microtubule (PVM) neurons was observed and compared in day 1 adults. PLM neurons had a long straight axon along the body in wild-type cells (Figure 6a,b).

FIGURE 4 Motility of amyotrophic lateral sclerosis-associated KIF5A on microtubules. The motility of 10 nM KIF5A::mSca, 10 nM KIF5A(Δ exon27)::mSca, 10 nM KIF5A::mSca-KLC1 complex, and 10 nM KIF5A(Δ exon27)::mSca-KLC1 complex on microtubules in the presence of 2 mM ATP was observed by TIRF microscopy. Wild-type protein from the blue shaded fraction and Δ exon27 protein from the red shaded fraction in Figure 3a,b were observed. (a) Representative TIRF images of KIF5A (magenta) and microtubules (cyan). Note that KIF5A(Δ exon27)::mSca and KIF5A(Δ exon27)::mSca-KLC1 bound to microtubules more frequently than KIF5A::mSca and KIF5A::mSca-KLC1. Bars, 10 μ m. (b) Representative kymographs of KIF5A::mSca, KIF5A(Δ exon27)::mSca, KIF5A::mSca-KLC1 complex, and KIF5A (Δ exon27)::mSca-KLC1 complex. Scale bars represent 10 s (vertical) and 10 μ m (horizontal). (c) Dot plots showing the landing rates of KIF5A::mSca (wt), KIF5A(Δ exon27)::mSca (Δ exon27), KIF5A::mSca-KLC1 complex (wt + KLC1), and KIF5A(Δ exon27)::mSca-KLC1 complex (Δ exon27 + KLC1). The number of KIF5A oligomers that bound to microtubules was counted and adjusted by the time window, microtubule length, and concentration. Each dot shows one data point. $N = 20$ kymographs from each sample. Data were analyzed by Brown–Forsythe and Welch ANOVA followed by Dunnett’s multiple comparisons test. ***, adjusted p value $< .001$. ****, adjusted p value $< .0001$. (d) Dot plots showing the run length of KIF5A(Δ exon27)::mSca (Δ exon27) and KIF5A(Δ exon27)::mSca-KLC1 complex (Δ exon27 + KLC1). $N = 202$ (Δ exon27) and 201 (Δ exon27 + KLC1). Data were analyzed with the Mann–Whitney test. ns, adjusted p value $> .05$ and not statistically significant. (e and f) Gaussian fit and histogram showing the velocity of KIF5A(Δ exon27) and the KIF5A (Δ exon27)::mSca-KLC1 complex (377 \pm 107 nm/sec (KIF5A(Δ exon27)) and 378 \pm 111 nm/sec (KIF5A(Δ exon27)-KLC1)). The means \pm standard deviation were obtained from best-fit values. $N = 349$ and 337, respectively. The velocity of KIF5A(Δ exon27) was not affected by KLC1. Note that a sufficient number of samples could not be collected for KIF5A(wt)::mSca and KIF5A(wt)::mSca-KLC1

The PVM neuron extends an axon that grows ventrally and then turns anteriorly when it reaches the ventral nerve cord (Figure 6a,b). No significant differences were found between KIF5A-expressing neurons and control neurons (Figure 6c). In contrast, KIF5A(Δ exon27)-

expressing neurons showed morphological defects (Figure 6d-f). Approximately 60% of worms showed abnormal PLM and PVM morphologies (Figure 6d), but no stereotypical abnormalities were found. The PLM cell body was often mislocalized, and some worms had

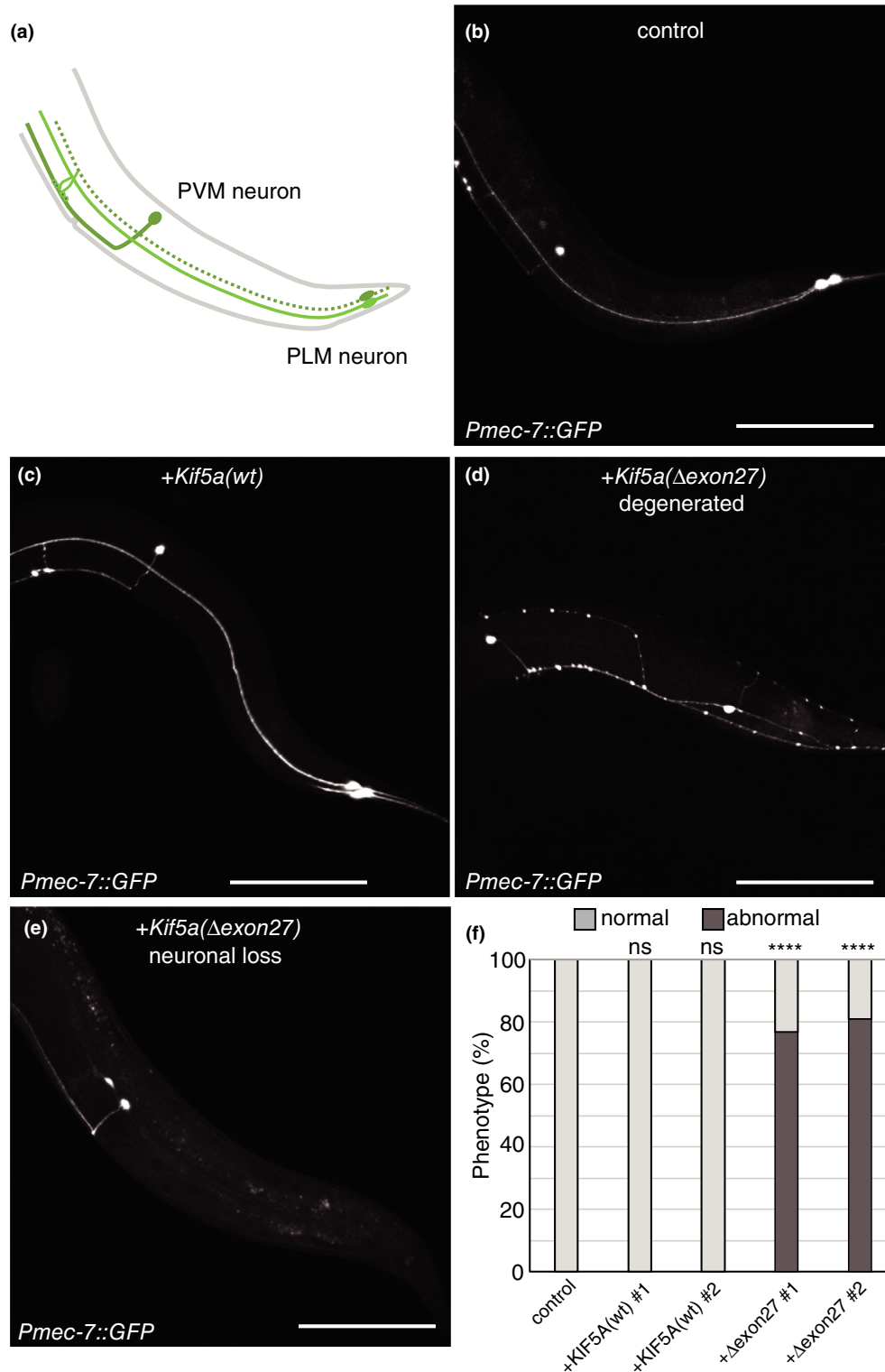


FIGURE 6 Legend on next page.

PLM neurons with multiple neuronal processes, whereas other worms had PLM neurons with bent axons. Approximately 20% of worms showed neuronal loss (Figure 6e). These data suggest that KIF5A (Δ exon27) is toxic in neurons.

3 | DISCUSSION

Previous studies have suggested that KIF5A (Δ exon27) causes ALS by a loss-of-function mechanism because the cargo-binding tail domain is deleted (Brenner et al., 2018; Nicolas et al., 2018). However, while several loss-of-function mutations have been found in the motor domain of KIF5A, these mutations cause SPG, rather than ALS (Ebbing et al., 2008; Reid et al., 2002). None of the motor domain mutations in KIF5A have been associated with ALS. These genetic data suggest that ALS mutations in KIF5A are not simple loss-of-function mutations. Protein aggregates are often associated with neurodegenerative disorders (Soto, 2003), and numerous ALS-associated mutations have been identified in other genes such as TARDBP (TDP-43 gene), SOD, and FUS (Aoki et al., 1993; Kabashi et al., 2008; Kwiatkowski Jr. et al., 2009; Vance et al., 2009). These mutations commonly induce aggregates that are toxic in cells (Bruijn et al., 1998; Johnson et al., 2009; Kwiatkowski Jr. et al., 2009). Our data suggest that the Δ exon27 mutation in KIF5A induces toxic aggregates. Furthermore, while we were preparing this manuscript, a preprint supporting the same conclusion was posted on Biorxiv (Pant et al., 2022). The study showed that KIF5A (Δ exon27) causes aggregate formation in cultured cells and is toxic when expressed in *Drosophila*. The study also showed that unpurified KIF5A (Δ exon27) in cell lysates is more active than wild-type KIF5A. What induces the formation of KIF5A (Δ exon27) aggregates? It is possible that unidentified proteins bind to the abnormal C-terminus of KIF5A (Δ exon27) and induce hyperactivation and aggregation. However, our assays using

purified proteins strongly suggest that KIF5A (Δ exon27) is hyperactive and is predisposed to form aggregates without the involvement of other factors (Figures 3–5).

The Δ exon27 mutation induces hyperactivation of KIF5A. KIF5 is inhibited by KLC-dependent and independent autoinhibitory mechanisms (Chiba et al., 2022; Hackney & Stock, 2000; Verhey et al., 1998). Binding with cargo vesicles or cargo complexes unlock the autoinhibition. The binding of KIF5A (Δ exon27) onto microtubules is suppressed by KLC1 (Figure 4c), suggesting that KLC-dependent autoinhibitory mechanism works even in KIF5A (Δ exon27). Interestingly, the IAK motif is not affected by the Δ exon27 mutation (Figure 1b). It was shown that hydrophobic materials such as polystyrene beads and glass surface can mimic cargos and activate KIF5-KLC complex when they bind to the tail region (Vale et al., 1985). Δ exon27 mutation induces the formation of large oligomers (Figure 3a,b). Large KIF5A (Δ exon27) oligomers may mimic cargos and activate the motor. It is also possible that Δ exon27 mutation disrupts previously unknown autoinhibitory mechanisms.

What induces toxicity in neurons? Toxicity in worm neurons would help to clarify neurotoxic mechanisms. One possibility is that hyperactivated KIF5A changes the distribution of cargo organelles and induces cellular toxicity. We have shown that another kinesin, human KIF1A, is functional in worm neurons (Chiba et al., 2019). We show here KIF5A (Δ exon27) binds to the cargo-binding adaptor KLC1 (Figure 3c). Thus, cargo transport may be affected by KIF5A (Δ exon27) even in worm neurons. Another possibility is that cargo transport is not directly related and KIF5A (Δ exon27) aggregates are toxic in neurons as is the case in other ALS-associated mutations (Bruijn et al., 1998; Johnson et al., 2009; Kwiatkowski Jr. et al., 2009). Aggregates change cellular metabolisms and induces neuronal death (Soto, 2003). These possibilities will be discriminated by analyzing cargo transport and distributions in KIF5A (Δ exon27)-expressed worm neurons. If aggregates

FIGURE 6 Neuronal toxicity in *Caenorhabditis elegans*. Human KIF5A or KIF5A (Δ exon27) was expressed in a *C. elegans* strain expressing green fluorescent protein (GFP) in mechanosensory neurons. (a and b) Morphology of posterior ventral microtubule (PVM) and posterior lateral microtubule (PLM) mechanosensory neurons. A schematic drawing of PVM and PLM neurons (a) and a representative image (b) of PVM and PLM neurons visualized by GFP expressed under the *mec-7* promoter (*Pmec-7*) are shown. (c–e) Representative images showing *Kif5a*-expressing mechanosensory neurons (c) and *Kif5a* (Δ exon27)-expressing neurons (d and e). (d) The formation of beads along the axon, an injured axon marker, is seen. Moreover, the cell body of PLM neuron is anteriorly mislocalized. The axon of PLM neuron abnormally bends while the axon of PVM turns posteriorly. (e) PLM neuron is lost. Bars, 100 μ m. (f) *C. elegans* phenotypes were classified according to mechanosensory neuron morphology into two categories: normal morphology (light gray) and abnormal morphology (dark gray), and the number of worms in each category was counted. $N = 87$ (control strain), 68 (KIF5A(wt)-expressing strain #1), 75 (KIF5A(wt)-expressing strain #2), 73 (KIF5A (Δ exon27)-expressing strain #1), and 79 (KIF5A (Δ exon27)-expressing strain #2). Data were analyzed with a chi-square test with Bonferroni correction. ns, adjusted p value $>.05$ and not statistically significant, ****, adjusted p value $<.0001$; compared with the control strain

are toxic, hyperactivation of KIF5A motor may enhance the toxicity because hyperactivation causes misaccumulation of KIF5A at axonal tips, leading to a high concentration of KIF5A and aggregate formation. This hypothesis is supported by the observation that KIF5A (Δ exon27) aggregates were often found at neurite tips in CAD cells (Figure 1).

We have previously shown that KIF5A forms more oligomers than KIF5B and KIF5C in vitro (Chiba et al., 2022). Additionally, KIF5A oligomers are more active than KIF5A dimers. However, the physiological significance of these phenomena remains elusive. We show here that even wild-type KIF5A has a propensity to form more aggregates in the cell than KIF5B (Figure 1). A similar property has been found for TDP-43. TDP-43 is intrinsically aggregation-prone, which implies that it may be directly involved in the pathogenesis of sporadic ALS (Johnson et al., 2009). The propensity of KIF5A to oligomerize may be related to sporadic ALS and may be enhanced by ALS-associated KIF5A mutations.

4 | EXPERIMENTAL PROCEDURES

4.1 | Molecular biology

Polymerase chain reaction (PCR) was performed using KOD FX neo (TOYOBO) as described in the manual. Restriction enzymes were purchased from New England BioLabs Japan.

pAcbac1 plasmids containing human *KIF5A*(BC146670) human *KIF5B*(BC126281), and *KLC1* (BC008881) was described previously (Chiba et al., 2022).

To generate mScarlet::KIF5A and mScarlet::KIF5B expressing plasmids, pmScarletC1 plasmid was obtained from Addgene. KIF5A and KIF5B were amplified by PCR and transferred to pmScarletC1. To generate an EGFP::KIF5B expressing vector, EGFP was amplified from pEGFPN1::KIF1A (Niwa et al., 2008) and replaced with mScarlet by using AgeI and XhoI sites. Δ exon27 mutation was introduced by Gibson assembly. cDNA fragment encoding the mutated domain (Figure 1a) was synthesized by gBlocks (Integrated DNA Technologies Japan) and replaced with the wild-type fragment by Gibson assembly (Gibson et al., 2009). Plasmids used in this paper is described in Table S1. Key plasmids were deposited to Addgene.

4.2 | CAD cell experiments

CAD cells were obtained from European Collection of Cell Cultures and maintained as described (Qi et al., 1997). For

observation, cells were cultured on glass coverslips (Matsunami, Tokyo, Japan). Plasmid transfection was performed by Lipofectamine LTX (Thermo Fisher Scientific) as described in the manufacturer's manual. 24 hours after the transfection, mScarlet and GFP signals were observed under Zeiss Axio Observer inverted microscope equipped with LSM800 confocal unit (Carl Zeiss). $\times 40$ water immersion objective lens (Numerical Aperture: 1.1) was used for imaging. ZEN software (Carl Zeiss) was used to control the system.

4.3 | Purification of KIF5A

pAcbac plasmids were transformed to generate bacmid. Sf9 cells were maintained as a suspension culture in Sf-900II serum-free medium (Thermo Fisher Scientific) at 27°C. To prepare baculovirus, 1×10^6 cells of Sf9 cells were transferred to each well of a tissue-culture treated 6 well plate. After the cells attached to the bottom of the dishes, about $\sim 5 \mu\text{g}$ of bacmid were transfected using 6 μl of Cellfectin II reagent (Thermo Fisher Scientific). Five days after initial transfection, the culture media were collected and spun at 3000 g for 3 min to obtain the supernatant (P1). For protein expression, 400 ml of Sf9 cells (2×10^6 cells/ml) were infected with 100 μl of P1 virus and cultured for 65 hr at 27°C. Cells were harvested and resuspended in 25 ml of lysis buffer (50 mM HEPES-KOH, pH 7.5, 150 mM KCH₃COO, 2 mM MgSO₄, 1 mM EGTA, 10% glycerol) along with 1 mM DTT, 1 mM PMSF, 0.1 mM ATP and 0.5% TritonX-100. After incubating on ice for 10 min, the lysates were centrifuged at 15,000 g for 20 min at 4°C. The resulting supernatant were subject to affinity chromatography described below.

For affinity chromatography, the supernatants were put over a column of Streptactin XT resin (IBA) at 4°C. The columns were then washed with excess lysis buffer to remove unbound material and the proteins were eluted in lysis buffer containing 100 mM D-biotin. Eluted proteins were further purified via size exclusion chromatography using a Superose 6 10/300 GL column (Cytiva) equilibrated in lysis buffer. Fractions containing the proteins were combined and concentrated on amicon spin filters with a 50 kDa cutoff. Concentrated proteins were frozen in LiN₂ and stored at -80°C .

4.4 | TIRF single-molecule motility assays

TIRF assays were performed as described (Chiba et al., 2019). Tubulin was purified from porcine brain as described (Castoldi & Popov, 2003). Tubulin was labeled

with Biotin-PEG₂-NHS ester (Tokyo Chemical Industry) and AZDye647 NHS ester (Fluoroprobes) as described (Al-Bassam, 2014). To polymerize Taxol-stabilized microtubules labeled with biotin and AZDye647, 30 μ M unlabeled tubulin, 1.5 μ M biotin-labeled tubulin and 1.5 μ M AZDye647-labeled tubulin were mixed in BRB80 buffer supplemented with 1 mM GTP and incubated for 15 min at 37°C. Then, an equal amount of BRB80 supplemented with 40 μ M taxol was added and further incubated for more than 15 min. The solution was loaded on BRB80 supplemented with 300 mM sucrose and 20 μ M taxol and ultracentrifuged at 100,000 g for 5 min at 30°C. The pellet was resuspended in BRB80 supplemented with 20 μ M taxol. Glass chambers were prepared by acid washing as previously described (McKenney et al., 2014). Glass chambers were coated with PLL-PEG-biotin (SuSoS). Polymerized microtubules were flowed into streptavidin adsorbed flow chambers and allowed to adhere for 5–10 min. Unbound microtubules were washed away using assay buffer [90 mM Hepes pH 7.4, 50 mM KCH₃COO, 2 mM Mg(CH₃COO)₂, 1 mM EGTA, 10% glycerol, 0.1 mg/ml biotin-BSA, 0.2 mg/ml kappa-casein, 0.5% Pluronic F127, 2 mM ATP, and an oxygen scavenging system composed of PCA/PCD/Trolox. Purified motor protein was diluted to indicated concentrations in the assay buffer. Then, the solution was flowed into the glass chamber. An ECLIPSE Ti2-E microscope equipped with a CFI Apochromat TIRF 100XC Oil objective lens, an Andor iXion life 897 camera and a Ti2-LAPP illumination system (Nikon) was used to observe single molecule motility. NIS-Elements AR software ver. 5.2 (Nikon) was used to control the system.

4.5 | Worm experiments and strains

C. elegans strains were maintained as described previously (Brenner, 1974). Wild-type worm N2 and feeder bacteria OP50 were obtained from *C. elegans* genetic center (CGC; Minneapolis). Nematode Growth Media (NGM) agar plates were prepared as described (S. Brenner, 1974). Transformation of *C. elegans* was performed by DNA injection as described (Mello et al., 1991). 5 ng of *Pmec-7::KIF5A* or *Pmec-7::KIF5A(Δ exon27)* plasmids were injected. Strains used in this study are described in Table S2.

Analysis of mechanosensory neurons in *Caenorhabditis elegans*

Mechanosensory neurons were visualized using *uIs31 [Pmec-7::gfp]* marker that was obtained from *C. elegans* genetic center (Chalfie et al., 1994). Strains expressing

human KIF5A or KIF5A(Δ exon27) were observed under Zeiss Axio Observer inverted microscope equipped with LSM800 confocal unit (Carl Zeiss). \times 20 objective lens (Numerical Aperture: 0.8) was used for imaging. ZEN software (Carl Zeiss) was used to control the system. Fiji was used to analyze image files (Schindelin et al., 2012).

AUTHOR CONTRIBUTIONS

S.N. designed the study; J.N., K.C., and S.N. performed the study; J.N., K.C., and S.N. analyzed the data; J.N., K.C., and S.N. wrote the paper.

ACKNOWLEDGMENTS

We thank all of the members of the McKenney lab (UC Davis), Sugimoto lab (Tohoku University), and Niwa lab (Tohoku University) for helpful discussions. SN was supported by JSPS KAKENHI (20H03247, 19H04738, 20K21378), the Kato Memorial Bioscience Foundation, and Takeda Science Foundation. KC was supported by Uehara Memorial Foundation, JSPS KAKENHI (21K20621) and MEXT Leading Initiative for Excellent Researchers (JPMXS0320200156). Some *C. elegans* strains and OP50 were obtained from the CGC. We thank Lisa Kreiner, PhD, from Edanz (<https://www.jp.edanz.com/ac>) for editing a draft of this manuscript.

CONFLICT OF INTEREST

The authors have no conflicts of interest directly relevant to the content of this article.

ORCID

Shinsuke Niwa  <https://orcid.org/0000-0002-8367-9228>

REFERENCES

- Al-Bassam, J. (2014). Reconstituting dynamic microtubule polymerization regulation by TOG domain proteins. *Methods in Enzymology*, 540, 131–148. <https://doi.org/10.1016/B978-0-12-397924-7.00008-X>
- Aoki, M., Ogasawara, M., Matsubara, Y., Narisawa, K., Nakamura, S., Itoyama, Y., & Abe, K. (1993). Mild ALS in Japan associated with novel SOD mutation. *Nature Genetics*, 5(4), 323–324. <https://doi.org/10.1038/ng1293-323>
- Boyle, L., Rao, L., Kaur, S., Fan, X., Mebane, C., Hamm, L., Thornton, A., Ahrends, J. T., Anderson, M. P., Christodoulou, J., Gennerich, A., Shen, Y., & Chung, W. K. (2021). Genotype and defects in microtubule-based motility correlate with clinical severity in KIF1A-associated neurological disorder. *HGG Adv*, 2(2), 100026. <https://doi.org/10.1016/j.xhgg.2021.100026>
- Brenner, D., Yilmaz, R., Muller, K., Grehl, T., Petri, S., Meyer, T., Grosskreutz, J., Weydt, P., Ruf, W., Neuwirth, C., Weber, M., Pinto, S., Claeys, K. G., Schrank, B., Jordan, B., Knehr, A., Gunther, K., Hubers, A., Zeller, D., ... German, A. L. S. n. M. N. D. N. E. T. German ALS network MND-NET. (2018). Hot-spot KIF5A mutations cause familial ALS. *Brain*, 141(3), 688–697. <https://doi.org/10.1093/brain/awx370>

- Brenner, S. (1974). The genetics of *Caenorhabditis elegans*. *Genetics*, 77(1), 71–94. <https://www.ncbi.nlm.nih.gov/pubmed/4366476>
- Brujijn, L. I., Houseweart, M. K., Kato, S., Anderson, K. L., Anderson, S. D., Ohama, E., Reaume, A. G., Scott, R. W., & Cleveland, D. W. (1998). Aggregation and motor neuron toxicity of an ALS-linked SOD1 mutant independent from wild-type SOD1. *Science*, 281(5384), 1851–1854. <https://doi.org/10.1126/science.281.5384.1851>
- Budaitis, B. G., Jariwala, S., Rao, L., Yue, Y., Sept, D., Verhey, K. J., & Gennerich, A. (2021). Pathogenic mutations in the kinesin-3 motor KIF1A diminish force generation and movement through allosteric mechanisms. *The Journal of Cell Biology*, 220(4), e202004227. <https://doi.org/10.1083/jcb.202004227>
- Castoldi, M., & Popov, A. V. (2003). Purification of brain tubulin through two cycles of polymerization-depolymerization in a high-molarity buffer. *Protein Expression and Purification*, 32(1), 83–88. [https://doi.org/10.1016/S1046-5928\(03\)00218-3](https://doi.org/10.1016/S1046-5928(03)00218-3)
- Chalfie, M., Tu, Y., Euskirchen, G., Ward, W. W., & Prasher, D. C. (1994). Green fluorescent protein as a marker for gene expression. *Science*, 263(5148), 802–805. <https://doi.org/10.1126/science.8303295>
- Chiba, K., Ori-McKenney, K. M., Niwa, S., & McKenney, R. J. (2022). Synergistic autoinhibition and activation mechanisms control Kinesin-1 motor activity. *Cell Rep*, in press.
- Chiba, K., Takahashi, H., Chen, M., Obinata, H., Arai, S., Hashimoto, K., Oda, T., McKenney, R. J., & Niwa, S. (2019). Disease-associated mutations hyperactivate KIF1A motility and anterograde axonal transport of synaptic vesicle precursors. *Proceedings of the National Academy of Sciences of the United States of America*, 116(37), 18429–18434. <https://doi.org/10.1073/pnas.1905690116>
- Coy, D. L., Hancock, W. O., Wagenbach, M., & Howard, J. (1999). Kinesin's tail domain is an inhibitory regulator of the motor domain. *Nature Cell Biology*, 1(5), 288–292. <https://doi.org/10.1038/13001>
- Ebbing, B., Mann, K., Starosta, A., Jaud, J., Schols, L., Schule, R., & Woehlke, G. (2008). Effect of spastic paraplegia mutations in KIF5A kinesin on transport activity. *Human Molecular Genetics*, 17(9), 1245–1252. <https://doi.org/10.1093/hmg/ddn014>
- Friedman, D. S., & Vale, R. D. (1999). Single-molecule analysis of kinesin motility reveals regulation by the cargo-binding tail domain. *Nature Cell Biology*, 1(5), 293–297. <https://doi.org/10.1038/13008>
- Gallegos, M. E., & Bargmann, C. I. (2004). Mechanosensory neurite termination and tiling depend on SAX-2 and the SAX-1 kinase. *Neuron*, 44(2), 239–249. <https://doi.org/10.1016/j.neuron.2004.09.021>
- Ghosh-Roy, A., Goncharov, A., Jin, Y., & Chisholm, A. D. (2012). Kinesin-13 and tubulin posttranslational modifications regulate microtubule growth in axon regeneration. *Developmental Cell*, 23(4), 716–728. <https://doi.org/10.1016/j.devcel.2012.08.010>
- Gibson, D. G., Young, L., Chuang, R. Y., Venter, J. C., Hutchison, C. A., 3rd, & Smith, H. O. (2009). Enzymatic assembly of DNA molecules up to several hundred kilobases. *Nature Methods*, 6(5), 343–345. <https://doi.org/10.1038/nmeth.1318>
- Hackney, D. D. (1995). Highly processive microtubule-stimulated ATP hydrolysis by dimeric kinesin head domains. *Nature*, 377(6548), 448–450. <https://doi.org/10.1038/377448a0>
- Hackney, D. D., Levitt, J. D., & Wagner, D. D. (1991). Characterization of alpha 2 beta 2 and alpha 2 forms of kinesin. *Biochemical and Biophysical Research Communications*, 174(2), 810–815. Retrieved from <https://www.ncbi.nlm.nih.gov/pubmed/1825168>
- Hackney, D. D., & Stock, M. F. (2000). Kinesin's IAK tail domain inhibits initial microtubule-stimulated ADP release. *Nature Cell Biology*, 2(5), 257–260. <https://doi.org/10.1038/35010525>
- Hall, D. H., & Hedgecock, E. M. (1991). Kinesin-related gene unc-104 is required for axonal transport of synaptic vesicles in *C. elegans*. *Cell*, 65(5), 837–847. [https://doi.org/10.1016/0092-8674\(91\)90391-b](https://doi.org/10.1016/0092-8674(91)90391-b)
- Harms, M. B., Ori-McKenney, K. M., Scoto, M., Tuck, E. P., Bell, S., Ma, D., Masi, S., Allred, P., Al-Lozi, M., Reilly, M. M., Miller, L. J., Jani-Acsadi, A., Pestronk, A., Shy, M. E., Muntoni, F., Vallee, R. B., & Baloh, R. H. (2012). Mutations in the tail domain of DYNC1H1 cause dominant spinal muscular atrophy. *Neurology*, 78(22), 1714–1720. <https://doi.org/10.1212/WNL.0b013e3182556c05>
- Hirokawa, N., Niwa, S., & Tanaka, Y. (2010). Molecular motors in neurons: Transport mechanisms and roles in brain function, development, and disease. *Neuron*, 68(4), 610–638. <https://doi.org/10.1016/j.neuron.2010.09.039>
- Hirokawa, N., Noda, Y., Tanaka, Y., & Niwa, S. (2009). Kinesin superfamily motor proteins and intracellular transport. *Nature Reviews. Molecular Cell Biology*, 10(10), 682–696. <https://doi.org/10.1038/nrm2774>
- Holzbaur, E. L., & Scherer, S. S. (2011). Microtubules, axonal transport, and neuropathy. *The New England Journal of Medicine*, 365(24), 2330–2332. <https://doi.org/10.1056/NEJMcibr1112481>
- Huynh, W., & Vale, R. D. (2017). Disease-associated mutations in human BICD2 hyperactivate motility of dynein-dynactin. *Journal of Cell Biology*, 216(10), 3051–3060. <https://doi.org/10.1083/jcb.201703201>
- Johnson, B. S., Snead, D., Lee, J. J., McCaffery, J. M., Shorter, J., & Gitler, A. D. (2009). TDP-43 is intrinsically aggregation-prone, and amyotrophic lateral sclerosis-linked mutations accelerate aggregation and increase toxicity. *The Journal of Biological Chemistry*, 284(30), 20329–20339. <https://doi.org/10.1074/jbc.M109.010264>
- Kabashi, E., Valdmanis, P. N., Dion, P., Spiegelman, D., McConkey, B. J., Vande Velde, C., Bouchard, J. P., Lacomblez, L., Pochigaeva, K., Salachas, F., Pradat, P. F., Camu, W., Meininger, V., Dupre, N., & Rouleau, G. A. (2008). TARDBP mutations in individuals with sporadic and familial amyotrophic lateral sclerosis. *Nature Genetics*, 40(5), 572–574. <https://doi.org/10.1038/ng.132>
- Kanai, Y., Dohmae, N., & Hirokawa, N. (2004). Kinesin transports RNA: Isolation and characterization of an RNA-transporting granule. *Neuron*, 43(4), 513–525. <https://doi.org/10.1016/j.neuron.2004.07.022>
- Kanai, Y., Okada, Y., Tanaka, Y., Harada, A., Terada, S., & Hirokawa, N. (2000). KIF5C, a novel neuronal kinesin enriched

- in motor neurons. *The Journal of Neuroscience*, 20(17), 6374–6384. <https://doi.org/10.1523/JNEUROSCI.20-17-06374.2000>
- Kardon, J. R., & Vale, R. D. (2009). Regulators of the cytoplasmic dynein motor. *Nature Reviews. Molecular Cell Biology*, 10(12), 854–865. <https://doi.org/10.1038/nrm2804>
- Kwiatkowski, T. J., Jr., Bosco, D. A., Leclerc, A. L., Tamrazian, E., Vanderburg, C. R., Russ, C., Davis, A., Gilchrist, J., Kasarskis, E. J., Munsat, T., Valdmanis, P., Rouleau, G. A., Hosler, B. A., Cortelli, P., de Jong, P. J., Yoshinaga, Y., Haines, J. L., Pericak-Vance, M. A., Yan, J., ... Brown, R. H., Jr. (2009). Mutations in the FUS/TLS gene on chromosome 16 cause familial amyotrophic lateral sclerosis. *Science*, 323(5918), 1205–1208. <https://doi.org/10.1126/science.1166066>
- McKenney, R. J., Huynh, W., Tanenbaum, M. E., Bhabha, G., & Vale, R. D. (2014). Activation of cytoplasmic dynein motility by dynactin-cargo adapter complexes. *Science*, 345(6194), 337–341. <https://doi.org/10.1126/science.1254198>
- Mello, C. C., Kramer, J. M., Stinchcomb, D., & Ambros, V. (1991). Efficient gene transfer in *C.elegans*: Extrachromosomal maintenance and integration of transforming sequences. *The EMBO Journal*, 10(12), 3959–3970. <https://www.ncbi.nlm.nih.gov/pubmed/1935914>
- Munch, C., Sedlmeier, R., Meyer, T., Homberg, V., Sperfeld, A. D., Kurt, A., Prudlo, J., Peraus, G., Hanemann, C. O., Stumm, G., & Ludolph, A. C. (2004). Point mutations of the p150 subunit of dynactin (DCTN1) gene in ALS. *Neurology*, 63(4), 724–726. <https://doi.org/10.1212/01.wnl.0000134608.83927.b1>
- Nakata, T., Niwa, S., Okada, Y., Perez, F., & Hirokawa, N. (2011). Preferential binding of a kinesin-1 motor to GTP-tubulin-rich microtubules underlies polarized vesicle transport. *The Journal of Cell Biology*, 194(2), 245–255. <https://doi.org/10.1083/jcb.201104034>
- Nicolas, A., Kenna, K. P., Renton, A. E., Ticozzi, N., Faghri, F., Chia, R., Dominov, J. A., Kenna, B. J., Nalls, M. A., Keagle, P., Rivera, A. M., van Rheenen, W., Murphy, N. A., van Vugt, J., Geiger, J. T., Van der Spek, R. A., Pliner, H. A., Shankaracharya, Smith, B. N., ... Landers, J. E. (2018). Genome-wide analyses identify KIF5A as a novel ALS gene. *Neuron*, 97(6), 1268–1283 e1266. <https://doi.org/10.1016/j.neuron.2018.02.027>
- Niwa, S., Tanaka, Y., & Hirokawa, N. (2008). KIF1Bbeta- and KIF1A-mediated axonal transport of presynaptic regulator Rab3 occurs in a GTP-dependent manner through DENN/MADD. *Nature Cell Biology*, 10(11), 1269–1279. <https://doi.org/10.1038/ncb1785>
- Okada, Y., Yamazaki, H., Sekine-Aizawa, Y., & Hirokawa, N. (1995). The neuron-specific kinesin superfamily protein KIF1A is a unique monomeric motor for anterograde axonal transport of synaptic vesicle precursors. *Cell*, 81(5), 769–780. Retrieved from <https://www.ncbi.nlm.nih.gov/pubmed/7539720>
- Pant, C. D., Parameswari, J., Rao, L., Shi, L., Chilukuri, G., McEachin, T. Z., Glass, J., Bassell, J. G., Gennerich, A., & Jiang, J. (2022). ALS-linked KIF5A ΔExon27 mutant causes neuronal toxicity through gain of function. *Biorxiv*. <https://doi.org/10.1101/2022.03.05.483071>
- Qi, Y., Wang, J. K., McMillian, M., & Chikaraishi, D. M. (1997). Characterization of a CNS cell line, CAD, in which morphological differentiation is initiated by serum deprivation. *The Journal of Neuroscience*, 17(4), 1217–1225. <https://doi.org/10.1523/JNEUROSCI.17-04-01217.1997>
- Reid, E., Kloos, M., Ashley-Koch, A., Hughes, L., Bevan, S., Svenson, I. K., Graham, F. L., Gaskell, P. C., Dearlove, A., Pericak-Vance, M. A., Rubinsztein, D. C., & Marchuk, D. A. (2002). A kinesin heavy chain (KIF5A) mutation in hereditary spastic paraplegia (SPG10). *American Journal of Human Genetics*, 71(5), 1189–1194. <https://doi.org/10.1086/344210>
- Schafheimer, N., & King, J. (2013). Tryptophan cluster protects human gammaD-crystallin from ultraviolet radiation-induced photoaggregation in vitro. *Photochemistry and Photobiology*, 89(5), 1106–1115. <https://doi.org/10.1111/php.12096>
- Schindelin, J., Arganda-Carreras, I., Frise, E., Kaynig, V., Longair, M., Pietzsch, T., Preibisch, S., Rueden, C., Saalfeld, S., Schmid, B., Tinevez, J. Y., White, D. J., Hartenstein, V., Eliceiri, K., Tomancak, P., & Cardona, A. (2012). Fiji: An open-source platform for biological-image analysis. *Nature Methods*, 9(7), 676–682. <https://doi.org/10.1038/nmeth.2019>
- Scholey, J. M. (2008). Intraflagellar transport motors in cilia: Moving along the cell's antenna. *The Journal of Cell Biology*, 180(1), 23–29. <https://doi.org/10.1083/jcb.200709133>
- Soto, C. (2003). Unfolding the role of protein misfolding in neurodegenerative diseases. *Nature Reviews. Neuroscience*, 4(1), 49–60. <https://doi.org/10.1038/nrn1007>
- Uchida, A., Alami, N. H., & Brown, A. (2009). Tight functional coupling of kinesin-1A and dynein motors in the bidirectional transport of neurofilaments. *Molecular Biology of the Cell*, 20(23), 4997–5006. <https://doi.org/10.1091/mbc.E09-04-0304>
- Vale, R. D. (2003). The molecular motor toolbox for intracellular transport. *Cell*, 112(4), 467–480. [https://doi.org/10.1016/s0092-8674\(03\)00111-9](https://doi.org/10.1016/s0092-8674(03)00111-9)
- Vale, R. D., Funatsu, T., Pierce, D. W., Romberg, L., Harada, Y., & Yanagida, T. (1996). Direct observation of single kinesin molecules moving along microtubules. *Nature*, 380(6573), 451–453. <https://doi.org/10.1038/380451a0>
- Vale, R. D., Reese, T. S., & Sheetz, M. P. (1985). Identification of a novel force-generating protein, kinesin, involved in microtubule-based motility. *Cell*, 42(1), 39–50. <https://www.ncbi.nlm.nih.gov/pubmed/3926325>
- Vance, C., Rogelj, B., Hortobagyi, T., De Vos, K. J., Nishimura, A. L., Sreedharan, J., Hu, X., Smith, B., Ruddy, D., Wright, P., Ganesalingam, J., Williams, K. L., Tripathi, V., Al-Saraj, S., Al-Chalabi, A., Leigh, P. N., Blair, I. P., Nicholson, G., de Belleruche, J., ... Shaw, C. E. (2009). Mutations in FUS, an RNA processing protein, cause familial amyotrophic lateral sclerosis type 6. *Science*, 323(5918), 1208–1211. <https://doi.org/10.1126/science.1165942>
- Verhey, K. J., Lizotte, D. L., Abramson, T., Barenboim, L., Schnapp, B. J., & Rapoport, T. A. (1998). Light chain-dependent regulation of kinesin's interaction with microtubules. *The Journal of Cell Biology*, 143(4), 1053–1066. <https://doi.org/10.1083/jcb.143.4.1053>
- Weedon, M. N., Hastings, R., Caswell, R., Xie, W., Paszkiewicz, K., Antoniadi, T., Williams, M., King, C., Greenhalgh, L., Newbury-Ecob, R., & Ellard, S. (2011). Exome sequencing identifies a DYNC1H1 mutation in a large pedigree with dominant axonal Charcot-Marie-tooth disease. *American Journal of*

Human Genetics, 89(2), 308–312. <https://doi.org/10.1016/j.ajhg.2011.07.002>

- Xia, C. H., Roberts, E. A., Her, L. S., Liu, X., Williams, D. S., Cleveland, D. W., & Goldstein, L. S. (2003). Abnormal neurofilament transport caused by targeted disruption of neuronal kinesin heavy chain KIF5A. *The Journal of Cell Biology*, 161(1), 55–66. <https://doi.org/10.1083/jcb.200301026>
- Zhao, C., Takita, J., Tanaka, Y., Setou, M., Nakagawa, T., Takeda, S., Yang, H. W., Terada, S., Nakata, T., Takei, Y., Saito, M., Tsuji, S., Hayashi, Y., & Hirokawa, N. (2001). Charcot-Marie-tooth disease type 2A caused by mutation in a microtubule motor KIF1Bbeta. *Cell*, 105(5), 587–597. [https://doi.org/10.1016/s0092-8674\(01\)00363-4](https://doi.org/10.1016/s0092-8674(01)00363-4)

SUPPORTING INFORMATION

Additional supporting information may be found in the online version of the article at the publisher's website.

How to cite this article: Nakano, J., Chiba, K., & Niwa, S. (2022). An ALS-associated KIF5A mutant forms oligomers and aggregates and induces neuronal toxicity. *Genes to Cells*, 27(6), 421–435. <https://doi.org/10.1111/gtc.12936>